Diamagnetic and paramagnetic shifts in self-assembled InAs lateral quantum dot molecules

Xinran Zhou, Miquel Royo, Weiwen Liu, Jihoon H. Lee, Gregory J. Salamo, Juan I. Climente, and Matthew F. Doty

Phys. Rev. B **91**, 205427 — Published 19 May 2015

DOI: 10.1103/PhysRevB.91.205427

Diamagnetic and paramagnetic shifts in self-assembled InAs lateral quantum dot molecules

Xinran Zhou[1], Miquel Royo[2], Weiwen Liu[1], Jihoon H. Lee[3,4], Gregory. J. Salamo[4], Juan I. Climente[2], and Matthew F. Doty[1*]
[1]*Department of Materials Science and Engineering, University of Delaware, Newark, DE 19716, USA*
[2]*Departament de Quimica Fisica i Analitica, Universitat Jaume I, E-12080, Castello, Spain*
[3]*School of Electronics and Information, Kwangwoon University, Nowon-gu, Seoul 139-701, South Korea and*
[4]*Institute of Nanoscale Science and Engineering, University of Arkansas, Fayetteville, Arkansas 72701, USA*
(Dated: today)

We uncover the underlying physics that explains the energy shifts of discrete states of individual InAs lateral quantum dot molecules (LQDMs) as a function of magnetic fields applied in the Faraday geometry. We observe that ground states of the LQDM exhibit a diamagnetic shift while excited states exhibit a paramagnetic shift. We explain the physical origin of the transition between these two behaviors by analyzing the molecular exciton states with effective mass calculations. We find that charge carriers in delocalized molecular states can become localized in single QDs with increasing magnetic field. We further show that the net effects of broken symmetry of the molecule and Coulomb correlation lead to the paramagnetic response.

PACS numbers: 78.67.Hc, 71.35.Ji, 78.20.Ls, 78.55.Cr

I. INTRODUCTION

Self-assembled quantum dots (QDs) are of great interest for both fundamental studies of confined electronic states and applications in next-generation optoelectronic devices.[1–3] Molecules composed of two or more QDs are analogous to "natural" molecules in that delocalized molecular states with unique properties can be created by coherent tunneling between the "atomic" constituents.[4–15] Unlike natural molecules, the molecular states of quantum dot molecules (QDMs) can be tailored during growth or manipulated *in situ* with applied electric, magnetic and optical fields. These properties make QDMs particularly interesting as components of future solid state optoelectronic devices.

Lateral QDMs (LQDMs) are composed of two quantum dots aligned side-by-side on the growth surface. Although the tunnel coupling in LQDMs is typically weaker than in vertical QDMs (dots stacked along the growth direction), LQDMs are compatible with the creation of devices that simultaneously manipulate inter-dot coupling and charge occupancy by applying electric fields in two dimensions.[16,17] Our previous spectroscopy and analysis of single LQDMs has revealed distinct spectral patterns that are characteristic of LQDMs with nearly-degenerate and non-degenerate "atomic" consituents.[15] These results agree with prior computational and experimental work that suggests the existence of delocalized molecular states under certain conditions.[18–23] Here we report the observation of diamagnetic shifts for carriers confined in the ground state of LQDMs and large paramagnetic shifts for carriers confined in the first excited state. We use effective mass models to explain the physical origins of this transition and show that the delocalized molecular states in the LQDMs are localized to single QDs by the magnetic field, substantially changing both the Coulomb interaction strengths and angular momentum of the charges in the LQDMs. As a result, the broken symmetry of the LQDM, relative to the near-circular symmetry of a single QD, enhances the paramagnetic response of the excited states. The results reveal new opportunities for "molecular engineering" in the solid state.

II. EXPERIMENTAL

The LQDMs we study are grown from single dome-shaped QDs that are partially covered and annealed. Anisotropic diffusion along the reconstructed [0 1 -1] crystal axis drives the formation of side-by-side InAs quantum dots connected by an In-rich basin.[24] The LQDMs are grown in a n-doped Schottky diode configuration and patterned with electrodes that apply an electric field along the growth direction to control the total charge occupancy of the LQDM.

We use magneto-optical spectroscopy to study both ground and excited states of individual LQDMs. The LQDM sample was held in an Advanced Research Systems DMX-20 cryostat for ensemble measurements and moved into a liquid Helium-cooled cryostat with a superconducting solenoid for measurement of PL from individual LQDMs as a function of magnetic field. The LQDMs are cooled to 8 K and subject to a magnetic field of up to 6 T in the Faraday geometry, i.e. the magnetic field is parallel to the optical axis and growth direction, but perpendicular to the molecular axis. The ensemble PL is excited by a Ti:sapphire laser at 860 nm with power density ranging from 71 W/cm^2 to 5 kW/cm^2. The PL signal is resolved with a 0.75 m spectrometer equipped with a liquid nitrogen cooled charge-coupled device (CCD) camera

using a diffraction grating with 150 grooves/ mm. The discrete PL lines from single LQDMs are excited by a diode laser at 890 nm with power density of 200 W/cm^2 and resolved with a CCD using a diffraction grating with 1200 grooves/ mm.

Fig. 1(b) shows the photoluminescence (PL) of an ensemble of LQDMs. Four distinct peaks, corresponding to emission from the ground states (GS) and first-through-third excited states (ES1-ES3) are observed at high excitation power. We note that the intensity of the GS relative to the ES is influenced by the wavelength sensitivity of our Si CCD camera. Multi-peak fitting of the ensemble PL reveals the energy separation between each energy shell; the GS and ES1 are typically separated by about 50 meV.

III. ENERGY SHELL STRUCTURES OF LQDMS

As reported previously, the ground states of confined electrons and holes of LQDMs are localized in individual QDs.[14,15] The first excited state for holes is largely localized, but the first excited state of electrons is delocalized over the LQDM. This electronic structure is schematically depicted in Fig. 1(a) and numerical calculations of the spatial extent of the carrier electronic density are presented in Fig. 4.

Previous work on this LQDM sample establishes that all of the observed PL lines originate in LQDMs rather than single QDs.[14,15] AFM images for an uncapped reference LQDM sample indicate that over 90% of the QD complexes are composed of two laterally aligned QDs. In the case that a single QD or clusters with more than two QDs are evolved, the PL energies of those QD configurations will be significantly different than the energies of two-QD LQDMs because the total amount of InAs in the QD complex is conserved during the evolution from single to double to multiple QDs. Because the size of the QD, limited by the volume of available InAs, determines the emission energy, we can rule out the possibility that PL in the spectral range we studied could have originated in structures other than 'diatomic' LQDMs.

Our prior work also establishes the existence of delocalized ES1 states for all LQDMs in this sample.[14,15] Although the degree of degeneracy of different LQDMs varies with the geometry and material composition of each LQDM, previous experimental and theoretical studies of the ES1 states of our LQDMs reveal that the existence of delocalized excited electron states is universal, regardless of the degeneracy of the neighboring QDs. The calculated exciton charge densities of LQDMs shown in Fig 7(b) also indicate that the delocalization of electrons still exists even if the inter-dot distance and energy difference are large (ΔE = 8 meV, d = 38 nm).

The black and red lines in Fig. 1(b) show discrete PL lines obtained from individual LQDMs. The time-integrated measurement approach allows the emission from higher-energy shells to be measured even at relatively low excitation power. The intensity of different PL peaks corresponds to the probability that the corresponding energy shell is occupied. We focus on the GS PL lines with higher-than-average energies to improve detection efficiency with our Si-based CCD. Emission from the GS and ES1 is easily distinguished by observing characteristic applied voltage and laser power dependence trends in the PL data.[14,15] A typical result for this power-dependent measurement is shown in Fig. 2(a). With increasing laser power density, the increase of the PL intensities of the three peaks with low energy (marked as G1, G2 and G3, see Fig. 2(b)) rise sub-linearly with a change in slope at a laser power density of approximately 125 W/cm^2. In contrast, the intensities of peaks in high-energy side (see Fig. 2(c)) increase superlinearly with increasing laser power. The different trends of these two groups of lines indicates that PL line G1, G2 and G3 are emitted from the ground shell of the LQDMs (GS) while

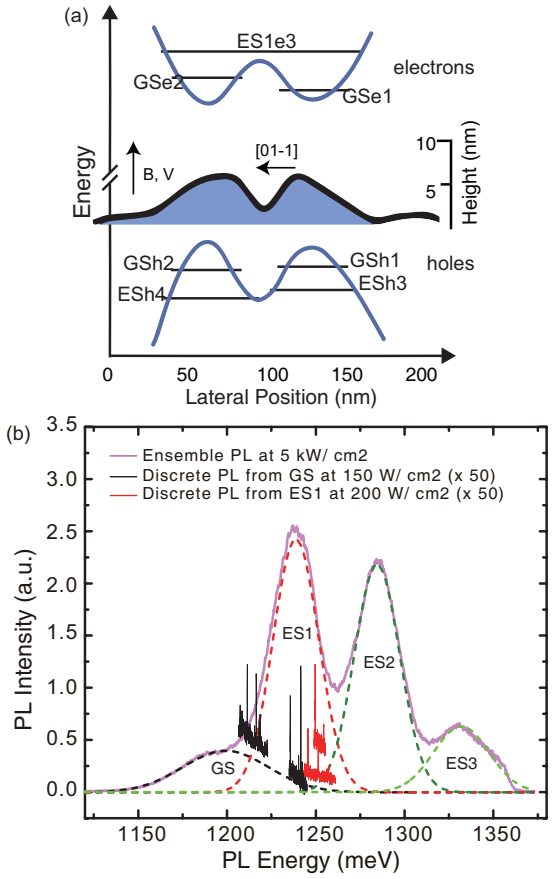

FIG. 1: (a) Schematic band diagram of a single LQDM. The middle inset shows the cross-sectional profile of a single LQDM with arrows denoting the molecular axis and the direction of applied electric and magnetic fields. (b) PL from LQDM ensemble (blue), single LQDM GSs (black) and single LQDM ES1s (red) measured in flat band conditions with zero magnetic field. The ensemble PL is fit by four Gaussian curves (dashed lines) to identify four PL energy shells.

E1, E2 and E3 are from the first excited shell (ES1).[14] We have also noticed that the Stark shift of PL lines in different shells varies. These two methods allow us to assign PL lines to specific energy shells.

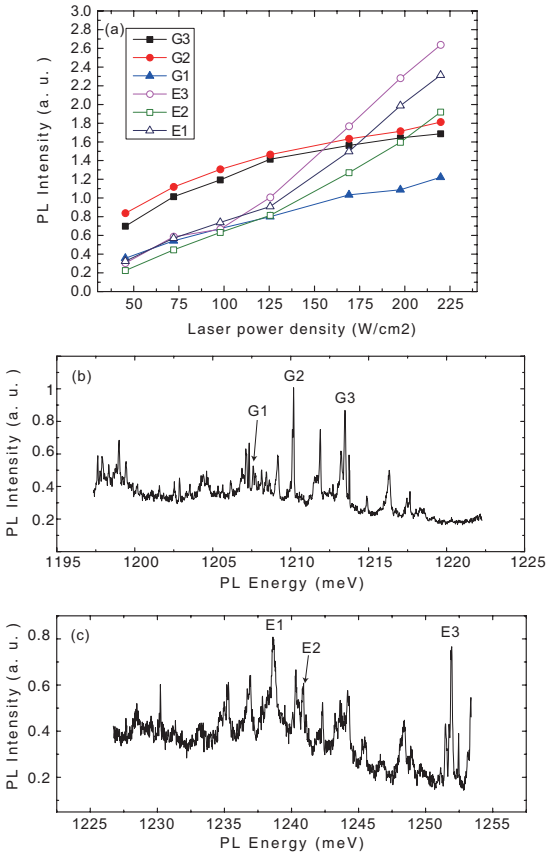

FIG. 2: (a) Dependence of photoluminescence intensity of discrete spectral lines emitted from LQDMs excited by a laser with power ranging from 50 to 225 W/cm^2. The PL peak labels correspond to discrete ground (b) or excited (c) states evident in the line spectra.

IV. ENERGY SHIFTS OF GS AND ES1 SHELLS UNDER MAGNETIC FIELDS

Fig. 3(a) shows the typical magnetic field dependence of PL emission from the GS and ES1, measured on two different LQDMs. The GS exhibits a 0.6 meV blue-shift as the magnetic field is increased to 6 T and a Zeeman splitting that reaches 0.3 meV. Over the same range of magnetic field ES1 exhibits a strong red shift (about 3.5 meV). Although the lines broaden slightly, no Zeeman splitting in the ES1 PL is observed within the range of magnetic fields studied. The continuous and smooth energy shifts and the full PL spectral maps (not shown) confirm that the number of charges in each LQDM does not change as a function of magnetic field.

The PL energy of QD ground states as a function of magnetic field is typically fit with an equation of the form:

$$E_{pl}(B) = E_{pl}(0) \pm b_{ex}B + a_{ex}B^2 \quad (1)$$

where $E_{pl}(0)$ is the PL energy at 0 T, b_{ex} is the linear coefficient and a_{ex} is the quadratic coefficient. Typically, in GS emissions, the linear term $\pm b_{ex}B$ corresponds to the Zeeman splitting and b_{ex} is given by $1/2\mu_B g_{ex}$, where g_{ex} is the exciton g factor and μ_B is the Bohr magneton. The quadratic term $a_{ex}B^2$ typically comes from the geometric confinement caused by the magnetic field and is referred to as the diamagnetic shift. By fitting the GS data in Fig. 3(a) with this equation, we are able to extract the linear and quadratic coefficients in a phenomenological way. For the PL emission of ES1, we set b_{ex} to zero because no Zeeman splitting is observed. In most of the ES1 PL lines no Zeeman splitting or broadening is observed. However, PL peak broadening with increasing magnetic field has been observed in several cases. This broadening could be related to Zeeman splitting that is below our spectral resolution. We do not have conclusive measurements or theory to address this point further. The fit value for a_{ex} is negative, in contrast to the positive value for the ground state PL. This negative a_{ex} quantifies the paramagnetic shift for the excited state that is evident in Fig. 3(a).

We apply the same fit to the magnetic-field dependent PL data of 25 distinct ground states and 23 distinct excited states of LQDMs. The values of a_{ex} returned by these fits are plotted in Fig. 3(b) as a function of PL energy. The average a_{ex} for GS PL (solid symbols) is 11.73 μeV/T^2 and the standard deviation is 4.27 μeV/T^2. This value is consistent with the diamagnetic coefficient observed for ground states of single InAs QDs and vertically-stacked QDMs.[25,26] The average value of a_{ex} for ES1 PL (open symbols), on the other hand, is -65.36 μeV/T^2, approximately 6 times larger in magnitude and opposite in sign. The standard deviation of a_{ex} in ES1 is 19.59 μeV/T^2. Red shifts of the excited state PL of single QDs , which have been well understood, originate in the circular symmetry of the single QD.[27,28] Unlike the well-localized charges in the GS, the wavefunction for charges in ES1 is better compared to the wavefunction for charges in quantum dots elongated along a certain lattice direction because of anisotropic growth.[29]The delocalized ES1 states in LQDMs do not have the circular symmetry of individual QDs and hence a new mechanism is required to explain the observed paramagnetic shifts.

V. THEORETICAL EXPLANATIONS

We now use single-band two-dimensional effective mass calculations to explain the physical origin of the pronounced red shift in the ES1 PL. We consider an exciton confined in the LQDM, described by the Hamiltonian

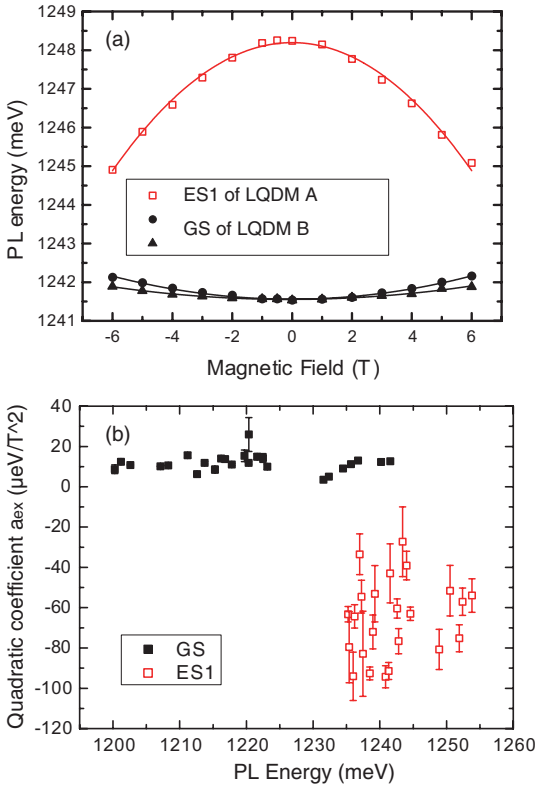

FIG. 3: (a) Energies of typical PL lines (GS, ES1) from two representative LQDMs as a function of magnetic field. (b) Diamagnetic coefficients for discrete PL lines from different energy shells of LQDMs as a function of PL energy.

$H_X = H_e + H_h + V_{eh}$. Here V_{eh} is the Coulomb interaction between electron and hole and H_e and H_h are the electron and hole single-particle Hamiltonians:

$$H_i = \frac{\mathbf{p}^2}{2\,m_i^*} - \frac{q_i B}{2\,m_i^*}\,L_z + \frac{(q_i B)^2}{8\,m_i^*}\,(x^2+y^2) + V_c^i, \qquad (2)$$

where m_i^* is the effective mass of the electron ($i = e$) or hole ($i = h$), q_i is the charge ($q_e = -1, q_h = 1$), B is the vertical magnetic field, $L_z = (xp_y - yp_x)$ the azimuthal angular momentum and V_c^i the confining potential. Hereafter we refer to the linear-in-B term of H_i as H_i^{B1}, and to the quadratic-in-B term as H_i^{B2}. We neglect the Zeeman effect, which is not relevant for determining the red shift of ES1. We use the same material parameters and confining potential that previously showed good agreement with experimental measurements of a nearly-degenerate LQDM from the same sample at zero magnetic field.[15]

The single-particle Hamiltonian (Eqn. 2) is integrated using three-point finite differences on a two-dimensional grid. The magnetic field is implemented with the symmetric gauge. Gauge invariance of the finite-difference discretization was checked by comparison with an alternative discretization formalism that averages the wave function in the B^2 term, as done e.g. in Ref. 30. The

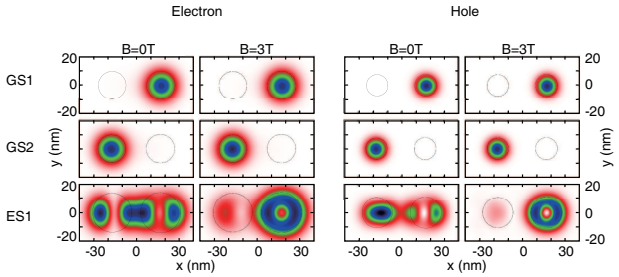

FIG. 4: Electron (left panels) and hole (right panels) charge densities corresponding to the three relevant exciton states at $B = 0$ T and $B = 3$ T. Dashed line circumferences depict the characteristic length of the harmonic oscillators defining each QD calculated for the electron and hole states with the largest contribution in the exciton wave function.

exciton Hamiltonian H_X is solved using a configuration interaction (CI) method in the basis formed from the 36 (48) lowest electron (hole) spin-orbitals. Coulomb integrals are obtained using the Fourier transform convolution theorem. The CI matrix is built and diagonalized using the CItool software.[33] The resulting exciton states are of the form $\Psi(\mathbf{r_e}, \mathbf{r_h}) = \sum c_{ij}\phi_i(\mathbf{r_e})\,\phi_j(\mathbf{r_h})$, where ϕ_n denotes a single-particle spin-oribtal.

The emission intensity is estimated within the dipolar approximation as proportional to the square of the electron-hole overlap, considering holes as complex-conjugated electrons,

$$I \propto |S_{eh}|^2 = \left| \sum_{ij} c_{ij} \int \phi_i(\mathbf{r_e})^* \phi_j(\mathbf{r_h})^* \delta(\mathbf{r_e} - \mathbf{r_h})\, d\mathbf{r_e}\, d\mathbf{r_h} \right|^2 . \qquad (3)$$

We note that considering a single exciton in excited states neglects quantitative corrections that may arise for ES1 PL due to the presence of additional excitons forming a closed shell in the lower-energy states. In single QDs such corrections have been estimated to be no more than 1 meV.[31]

We first compute the excitonic electron and hole charge densities in the two ground states (GS1 and GS2) and the first excited state (ES1). As shown in Fig. 4, at $B = 0$ T the GS charge densities of both electrons (left panels) and holes (right panels) are localized in individual QDs. For the first excited state, the hole is also mainly localized inside one QD (left dot), but the electron is clearly delocalized over the whole LQDM, forming a molecular orbital. This picture is consistent with that inferred in previous experiments on LQDM.[14] When the magnetic field is switched on, $B = 3$ T, the GS charges remain largely unaffected. By contrast, the excited electron becomes trapped into the right QD, and the hole follows behind bound by Coulomb interaction. In other words, the magnetic field turns off the molecular character of the excited state.

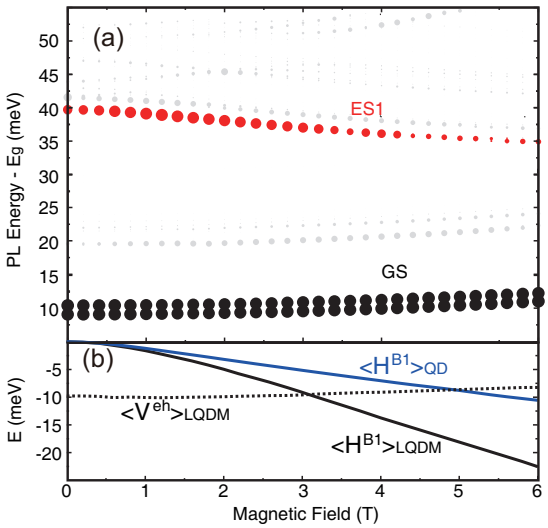

FIG. 5: (a) Exciton emission spectrum as a function of magnetic field. Black dots are used for GS1 and GS2, red dots for ES1 and gray dots for other non-relevant exciton states. The size of the dots is proportional to the optical intensity. (b) The expectation values of Coulomb interaction (dashed) and linear-in-B single-particle terms for a LQDM (solid black) and a QD (solid blue).

Next, we compute the exciton emission spectrum as a function of B. The result is shown in Fig. 5(a). Black dots are used for emission from the two GS, red dots for emission from ES1 and gray dots for other transitions (e.g., transitions involving highly excited hole states) The size of the dots indicates the optical intensity, estimated within the dipolar approach.[22] One can see that the theory captures qualitatively the magnetic response observed in Fig. 3, with a moderate diamagnetic shift of the GS transitions and a larger, non-linear paramagnetic shift of the optically active ES1 transitions.

As evident in Fig.5(a), it is straightforward to identify the quadratic-in-B term, H_e^{B2}, as the origin of the diamagnetic shift with increasing field in GS shells because L_z=0 in circular symmetry and the linear-in-B terms in Eq. (2) vanish. In contrast, for ES1 states H_e^{B2} is necessarily positive and L_z is not well-defined. There are two factors potentially responsible for the paramagnetic (red) shift of ES1: (1) an enhancement of the electron-hole Coulomb interaction, V_{eh}, as the increasing magnetic field localizes the electron into the same QD as the hole and (2) the linear-in-B single-particle terms, $H^{B1} = H_e^{B1} + H_h^{B1}$. To identify the physical origin of the paramagnetic shift we compare the expectation value of these two terms for the optically active ES1 exciton. The results, displayed in Fig. 5(b), clearly show that $\langle V_{eh}\rangle$ has a slight blue shift and the net red shift originates in the H^{B1} term.

VI. DISCUSSION

The above result is somewhat surprising in two senses. First, the Coulomb attraction gives no contribution to the paramagnetic shift (rather the opposite) in spite of B driving the electron and hole into the same QD. This is because the field lifts exciton quasi-degeneracies, thus reducing Coulomb correlations that helped increase electron-hole attraction. Second, it is not obvious that H^{B1} should give a red shift in an LQDM. H^{B1} does induce a red shift in single QDs with nearly circular symmetry,[28] but in such a case L_z is a good quantum number and the optically active p-shell exciton is mainly formed by an electron with $L_z^e = -1$ and a hole with $L_z^h = +1$. Both H_e^{B1} and H_h^{B1} contribute to the exciton red shift in a single QD, though H_e^{B1} is primarily responsible due to the lighter electron mass. In a LQDM, however, the symmetry is drastically lowered and the states have no well defined L_z. One may then expect $\langle L_z^e\rangle \approx 0$, which would suppress the paramagnetic shift, but we find exactly the opposite behavior. If we compare the red shift induced by $\langle H^{B1}\rangle$ for the LQDM and one of the constituent QDs alone (see Fig. 5(b)), the former is twice larger. In a single QD, $\langle L_z^e\rangle$ smoothly decreases from 0 to -1 atomic units as the magnetic field B increases (see red dots in Fig. 6). In contrast, $\langle L_z^e\rangle$ in the quasi-degenerate LQDM fluctuates and evolves from 0 towards negative values well under -1 (see blue dots in the figure). As a consequence, ES1 in the LQDM shows a pronounced red shift. The overall red shift is similar for single QD and LQDM because other terms like H_e^{B2} compensate.

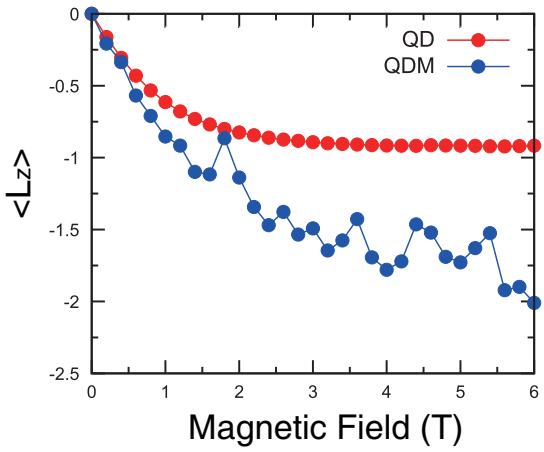

FIG. 6: Angular momentum expectation value for the electron in a p-shell exciton of a single QD (red dots) and that of a quasi-degenerate LQDM (blue dots). For the single QD $\hbar\omega = 25$ meV. For the LQDM $\hbar\omega_L = 23.5$ meV (left dot) and $\hbar\omega_R = 25.0$ meV (right dot). The distance between QD centers is 35 nm.

This behavior is explained as follows. The B-induced carrier localization into the QDs makes the LQDM emis-

sion spectrum resemble that of two individual, nearly degenerate QDs (cf. Fig. 5 with Fig. 2 of Ref. 32). At the same time, the lowered symmetry enables mixing between states which would otherwise have different L_z. In particular, for the electron it allows strong mixing between the states that eventually converge to the lowest Landau level, which in the single QD would have $L_z^e \leq 0$. As a result, $\langle L_z^e \rangle$ rapidly decreases with B.

The high areal density of LQDMs in our sample makes it impossible to conclusively assign ES1 PL to a LQDM with degenerate vs non-degenerate GS energies of the two constituent QDs. However, we can use theoretical models to estimate the influence of changing degeneracy. Fig. 7 shows the calculated exciton emission spectrum and exciton charge densities of LQDMs with different interdot spacing and degrees of degeneracy under magnetic field. Red dots are used to highlight the molecular exciton state. Although the spatial localization of charges in ES1 depends strongly on the inter-QD degeneracy, no significant change in the paramagnetic energy shifts is observed. The non-degenerate LQDMs can be considered as a system with properties between a single QD and a LQDM with nearly-degenerate constituent QDs. In non-degenerate LQDMs the increase of the angular momentum with increasing magnetic field is weaker than in quasi-degenerate LQDMs while the Coulomb attraction increases more quickly. The net effect of these two factors leads to a 5 meV energy shift when B=6 T regardless of the degree of degeneracy.

In conclusion, we used PL measurements of single LQDMs to observe the energy shift of discrete states as a function of applied magnetic field in the Faraday configuration. The red shift in the energy of first excited states is comparable to that observed for single QDs despite the broken circular symmetry of the LQDMs. We show that this red shift arises due to a competition between two effects: 1) the magnetic field localizes molecular states into the individual dots where coupling between states of the lowest Landau level leads to a significant increase of the angular momentum and a large red shift in state energy and 2) the magnetic field splits exciton states energetically, thus reducing Coulomb correlations and offseting the large red shift due to the angular momentum term. The fact that the molecular character of ES1 states can be switched on and off with applied magnetic fields, which can not be observed in single QDs or VQDMs, suggests that there may be new opportunities for manipulating the spatial extent of wavefunctions and coherent interactions between isolated quantum states. The results further suggest that the structural symmetry of QD molecules can be manipulated to tailor the optoelectronic and quantum properties of QD materials for next-generation device applications.

Acknowledgments

We thank J. Planelles for helpful discussions. The work was financially supported by NSF DMR-0844747 (XZ,MD), APOSTD/2013/052 GV VALi+d Grant (MR), NRF of Korea no. 2011-C0030821/ 2013R1A1A1007118 (JL), NSF DMR 1309989 (GS) and MINECO Project CTQ2011-27324 (JIC).

* Electronic address: doty@udel.edu

[1] A. J. Shields, Nature Photonics **1**, 215 (2007), ISSN 1749-4885, 166GV Times Cited:333 Cited References Count:102, URL <GotoISI>://WOS:000246367300011.

[2] R. J. Warburton, NATURE MATERIALS **12**, 483 (2013), ISSN 1476-1122.

[3] S. E. Economou, J. I. Climente, A. Badolato, A. S. Bracker, D. Gammon, and M. F. Doty, Physical Review B **86** (2012), ISSN 1098-0121 1550-235X.

[4] H. J. Krenner, M. Sabathil, E. C. Clark, A. Kress, D. Schuh, M. Bichler, G. Abstreiter, and J. J. Finley, Physical Review Letters **94**, 57402 (2005).

[5] E. A. Stinaff, M. Scheibner, A. S. Bracker, I. V. Ponomarev, V. L. Korenev, M. E. Ware, M. F. Doty, T. L. Reinecke, and D. Gammon, Science **311**, 636 (2006).

[6] A. S. Bracker, M. Scheibner, M. F. Doty, E. A. Stinaff, I. V. Ponomarev, J. C. Kim, L. J. Whitman, T. L. Reinecke, and D. Gammon, Applied Physics Letters **89**, 233110 (2006).

[7] M. F. Doty, M. Scheibner, I. V. Ponomarev, E. A. Stinaff, A. S. Bracker, V. L. Korenev, T. L. Reinecke, and D. Gammon, Physical Review Letters **97**, 197202 (2006).

[8] H. J. Krenner, E. C. Clark, T. Nakaoka, M. Bichler, C. Scheurer, G. Abstreiter, and J. J. Finley, Physical Review Letters **97**, 76403 (2006).

[9] M. F. Doty, M. Scheibner, A. S. Bracker, I. V. Ponomarev, T. L. Reinecke, and D. Gammon, Physical Review B **78**, 115316 (2008).

[10] M. F. Doty, J. I. Climente, M. Korkusinski, M. Scheibner, A. S. Bracker, P. Hawrylak, and D. Gammon, Physical Review Letters **102**, 47401 (2009).

[11] L. Wang, A. Rastelli, S. Kiravittaya, M. Benyoucef, and O. G. Schmidt, ADVANCED MATERIALS **21**, 2601 (2009), ISSN 0935-9648.

[12] W. Liu, S. Sanwlani, R. Hazbun, J. Kolodzey, A. S. Bracker, D. Gammon, and M. F. Doty, Phys. Rev. B **84**, 121304 (2011), URL http://link.aps.org/doi/10.1103/PhysRevB.84.121304.

[13] W. Liu, A. S. Bracker, D. Gammon, and M. F. Doty, Phys. Rev. B **87**, 195308 (2013), URL http://link.aps.org/doi/10.1103/PhysRevB.87.195308.

[14] X. Zhou, S. Sanwlani, W. Liu, J. H. Lee, Z. M. Wang, G. Salamo, and M. F. Doty, Phys. Rev. B **84**, 205411 (2011), URL http://link.aps.org/doi/10.1103/PhysRevB.84.205411.

[15] X. R. Zhou, J. H. Lee, G. J. Salamo, M. Royo, J. I. Climente, and M. F. Doty, Phys. Rev. B **87**, 125309 (2013), URL http://link.aps.org/doi/10.1103/PhysRevB.87.125309.

[16] G. Beirne, C. Hermannstadter, L. Wang, A. Rastelli, O. Schmidt, and P. Michler, PHYSICAL REVIEW LETTERS **96** (2006), ISSN 0031-9007.

[17] X. Zhou and M. Doty, Journal of Applied Physics **116**,

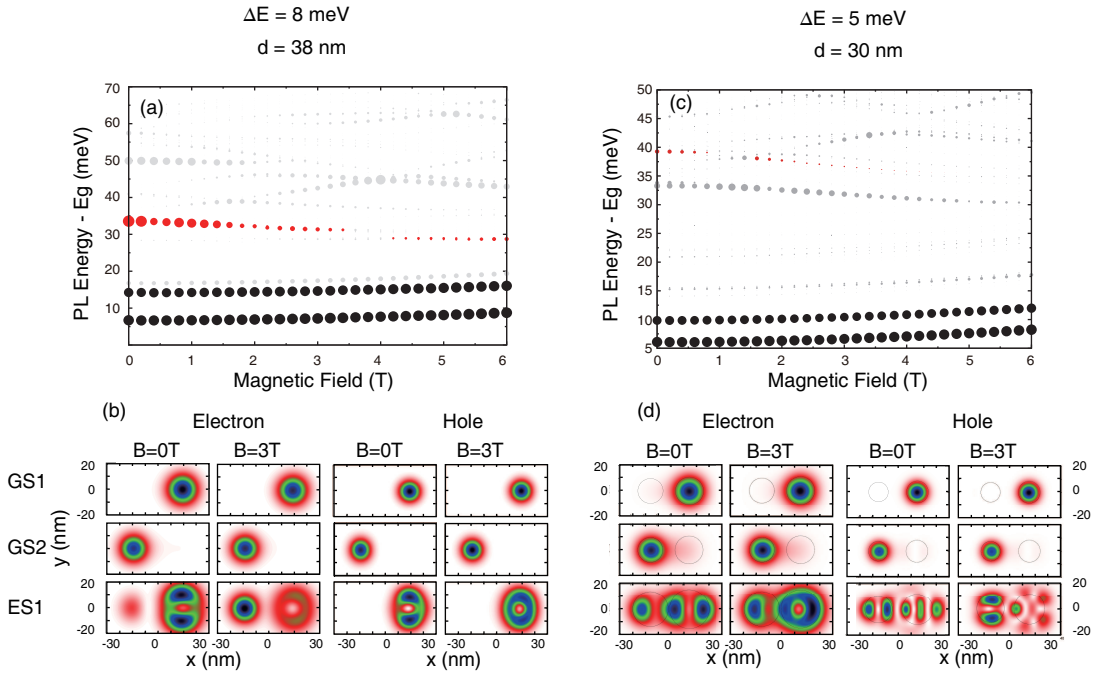

FIG. 7: Calculated exciton emission emission spectra (top row) and exciton charge densities (bottom row) of LQDMs with different degrees of degeneracy.

163101 (2014), ISSN 0021-8979 1089-7550.

[18] C. Hermannstadter, G. J. Beirne, M. Witzany, M. Heldmaier, J. Peng, G. Bester, L. Wang, A. Rastelli, O. G. Schmidt, and P. Michler, Physical Review B **82**, 085309 (2010).

[19] J. Peng, C. Hermannstadter, M. Witzany, M. Heldmaier, L. Wang, S. Kiravittaya, A. Rastelli, O. G. Schmidt, P. Michler, and G. Bester, Physical Review B **81**, 205315 (2010).

[20] J. Peng and G. Bester, Physical Review B Phys. Rev. B PRB **82**, 235314 (2010).

[21] G. Munoz-Matutano, M. Royo, J. I. Climente, J. Canet-Ferrer, D. Fuster, P. Alonso-Gonzalez, I. Fernandez-Martinez, J. Martinez-Pastor, Y. Gonzalez, L. Gonzalez, et al., Phys. Rev. B **84**, 041308 (2011).

[22] M. Royo, J. I. Climente, and J. Planelles, PHYSICAL REVIEW B **84** (2011), ISSN 1098-0121.

[23] M. Heldmaier, M. Seible, C. Hermannstaedter, M. Witzany, R. Rossbach, M. Jetter, P. Michler, L. Wang, A. Rastelli, and O. G. Schmidt, PHYSICAL REVIEW B **85** (2012), ISSN 1098-0121.

[24] J. Lee, Z. Wang, V. Dorogan, Y. Mazur, and G. Salamo, IEEE Transactions on Nanotechnology **9**, 149 (2010).

[25] S. Brown, T. Kennedy, D. Gammon, and E. Snow, Physical Review B **54**, R17339 (1996), ISSN 0163-1829 1095-3795.

[26] H. Kim, T. C. Shen, D. Sridharan, G. S. Solomon, and E. Waks, Applied Physics Letters **98**, 091102 (2011), ISSN 00036951.

[27] M. Bayer, A. Schmidt, A. Forchel, F. Faller, T. L. Reinecke, P. A. Knipp, A. A. Dremin, and V. D. Kulakovskii, Phys. Rev. Lett. **74**, 3439 (1995), URL `http://link.aps.org/doi/10.1103/PhysRevLett.74.3439`.

[28] S. Raymond, S. Studenikin, A. Sachrajda, Z. Wasilewski, S. J. Cheng, W. Sheng, P. Hawrylak, A. Babinski, M. Potemski, G. Ortner, et al., Phys. Rev. Lett. **92**, 187402 (2004), URL `http://link.aps.org/doi/10.1103/PhysRevLett.92.187402`.

[29] S. Hameau, Y. Guldner, O. Verzelen, R. Ferreira, G. Bastard, J. Zeman, A. Lemaitre, and J. M. Gerard, Phys. Rev. Lett. **83**, 4152 (1999), URL `http://link.aps.org/doi/10.1103/PhysRevLett.83.4152`.

[30] F. Gagel and K. Maschke, Phys. Rev. B **52**, 2013 (1995), URL `http://link.aps.org/doi/10.1103/PhysRevB.52.2013`.

[31] Y. Sidor, B. Partoens, F. M. Peeters, N. Schildermans, M. Hayne, V. V. Moshchalkov, A. Rastelli, and O. G. Schmidt, Phys. Rev. B **73**, 155334 (2006), URL `http://link.aps.org/doi/10.1103/PhysRevB.73.155334`.

[32] U. Hohenester and E. Molinari, physica status solidi (a) **178**, 277 (2000), ISSN 1521-396X, URL `http://dx.doi.org/10.1002/1521-396X(200003)178:1<277::AID-PSSA277>3.0.CO;2-A`.

[33] https://code.google.com/p/citool/